DOI: 10.1002/cbic.200800548

Assessing Carbohydrate–Carbohydrate Interactions by NMR Spectroscopy: The Trisaccharide Epitope from the Marine Sponge *Microciona prolifera*

J. Ignacio Santos,[a] Adriana Carvalho de Souza,[b] F. Javier Cañada,[a] Sonsoles Martín-Santamaría,*[c] Johannis P. Kamerling,*[b] and Jesús Jiménez-Barbero*[a]

Diffusion-ordered NMR spectroscopy (DOSY-NMR) and TR-NOESY-NMR experiments are used to detect ligand binding to macromolecular receptors. These techniques have been applied to detect weak carbohydrate–carbohydrate self-recognition in solution, making use of sugar-decorated gold nanoparticles as the "macromolecule" and the same carbohydrate as the ligand. Changes in the diffusion coefficient of the free carbohydrate in the presence of the glyconanoparticle (only with Ca^{II} ions in the sample solution), as well as changes in the sign of the sugar NOE peaks—positive for the free sugar (in the presence or absence of Ca^{II}) and negative for the sugar only in the simultaneous presence of the glyconanoparticle and Ca^{II} ions—have been taken as proof of weak Ca^{II}-mediated carbohydrate–carbohydrate interactions in solution. Although different methods such as SPR, TEM, and AFM have been used in the past to detect carbohydrate–carbohydrate interactions with the aid of gold nanoparticles and gold self-assembled monolayers, they are restricted to high-affinity ranges. The methods used in this study allow expansion of the number of techniques to tackle this relevant biological problem, also for approaching ligand–receptor interactions below the high-affinity range. Additionally, 3D models of trisaccharide-Ca^{II}-trisaccharide complexes based on results from molecular dynamics simulations are proposed.

Introduction

Molecular recognition events are at the heart of living systems. Depending on the chemical natures of the interacting moieties, different ranges of affinities are accessible; this allows distinct associated features to be studied. Cell recognition and adhesion involve many kinds of cell surface molecules that interact in homotypic and/or heterotypic ways.[1]

Cellular adhesion in marine sponges is an event mediated by species-specific extracellular proteoglycans, otherwise known as aggregation factors.[2] For the species-specific cell adhesion in the marine sponge *Microciona prolifera*, two highly polyvalent functional domains of its proteoglycan (MAF) are held responsible: MAF, the first circular proteoglycan described, is composed of two N-glycosylated proteins—MAFp3 and MAFp4—with twenty units of each glycoprotein forming the central ring and the radiating arms, respectively. Each MAFp3 unit carries one or two copies of a 200 kDa acidic glycan (g-200), whereas each MAFp4 carries about 50 copies of a 6 kDa glycan (g-6).[3] The MAFp4 arms of the sunburst-like proteoglycan are linked to cell-surface binding receptors, while the MAFp3 ring exposes the g-200 glycans so that they can engage in Ca^{II}-dependent self-association.[3]

Partial characterization of the g-200 glycan showed that it contained, among other fragments, two small oligosaccharide epitopes—the pyruvated trisaccharide Gal*p*4,6(*R*)Pyr(β1-4)-Glc*p*NAc(β1-3)Fuc*p* and the sulfated disaccharide Glc*p*NAc3*S*-(β1-3)Fuc*p* (D-configuration for Gal and GlcNAc; L-configuration for Fuc)—that play a role in the carbohydrate–carbohydrate interaction process.[4] Through the use of the synthetic sulfated disaccharide, multivalently presented as a bovine serum albumin conjugate, and surface plasmon resonance (SPR) spectroscopy it was shown that Ca^{II}-dependent carbohydrate self-recognition is a major force in the g-200 association phenomenon.[5] Recently, transmission electron microscopy (TEM) imaging of gold glyconanoparticles (GNPs) decorated with Glc*p*NAc3*S*(β1-3)Fuc*p*(α1-O)$(CH_2)_3$S$(CH_2)_6$SH and related structures, in the presence or absence of Ca^{II} ions, has provided valuable information about the mechanism of this Ca^{II}-dependent disaccharide self-recognition.[6,7] Atomic force microscopy (AFM) experiments showed a force quantum of 30 ± 6 pN for the interaction of a single disaccharide pair.[8] On the basis of these model studies it was postulated that after the coordination of Ca^{II} ions by several functional groups, the sulfated disaccharide would reach a suitable conformation in which other interactions, such as hydrophobic interactions, would take place to stabilize the entire complex (Scheme 1).

[a] *Dr. J. I. Santos, Dr. F. J. Cañada, Prof. Dr. J. Jiménez-Barbero*
Centro de Investigaciones Biológicas, CIB–CSIC
28040 Madrid (Spain)
E-mail: jjbarbero@cib.csic.es

[b] *Dr. A. Carvalho de Souza, Prof. Dr. J. P. Kamerling*
Bijvoet Center, Department of Bio-Organic Chemistry, Utrecht University
3584 CH Utrecht (The Netherlands)

[c] *Dr. S. Martín-Santamaría*
Departamento de Química, Facultad de Farmacia, Universidad San Pablo CEU, 28668 Boadilla del Monte, Madrid (Spain)

Supporting information for this article is available on the WWW under http://www.chembiochem.org or from the author.

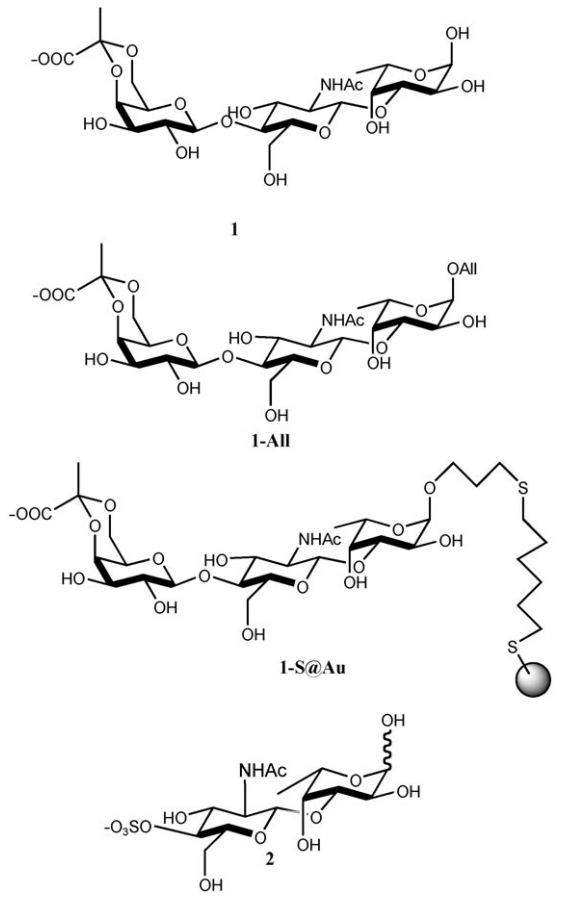

Scheme 1. Structures of the pyruvated trisaccharide (**1**) and the sulfated disaccharide (**2**) epitopes involved in the carbohydrate–carbohydrate self-recognition of the g-200 glycan.

The use of GNPs combined with TEM methodology, as successfully applied for the synthetic sulfated disaccharide, did not allow detection of self-assembly for the second putative oligosaccharide fragment: Gal*p*4,6(*R*)Pyr(β1-4)Glc*p*NAc(β1-3)-Fuc*p*(α1-.[8] It can be speculated that this is due to a lower affinity, which does not allow for detection of the interaction by TEM and AFM.

In the study of carbohydrate–carbohydrate interactions, it has been reported that two Le^X units can interact in the presence of Ca^{II} ions to form a Le^X-Ca^{II}-Le^X complex, as demonstrated by a variety of techniques.[9] Weak interactions with Ca^{II} have been detected by NMR for Le^X oligosaccharides tethered to lipid bilayers,[10] but Ca^{II}-induced complexation of Le^X glycoconjugates has not so far been observed in solution.

Current developments in NMR techniques have allowed examination of specificity, affinity, and structural aspects of receptor–ligand interaction.[11] Among the NMR methods suitable for analyzing ligand binding, transferred NOE[12] and DOSY[13,14] are particularly useful for detection of binding based on changes in the rotational (TR-NOESY) and translational (DOSY) properties of the ligands upon binding to large receptors. These techniques are particularly useful in the medium-to-low affinity range, and, therefore it is speculated on whether they could be adopted to detect weak-affinity carbohydrate–carbohydrate interactions such as those described above.

In this context, here we present a ^{1}H NMR-based approach to exploration of the existence of carbohydrate–carbohydrate interactions mediated by Ca^{II} ions in the case of the synthetic trisaccharide components Gal*p*4,6(*R*)Pyr(β1-4)Glc*p*NAc(β1-3)-Fuc*p*(α1-O)(CH_2CHCH_2) (**1-All**) and Gal*p*4,6(*R*)Pyr(β1-4)Glc*p*NAc-(β1-3)Fuc*p*(α1-O)$(CH_2)_3S(CH_2)_6$S@Au (**1-S@Au**).[8] Additionally, molecular dynamics (MD) simulations have been carried out to corroborate the experimental observations.

Results and Discussion

DOSY experiments

Diffusion ordered spectroscopy (DOSY) is a method for the determination of molecular size through the measurement of diffusion coefficients (log *D*). In the context of ligand–receptor interactions, the log *D* values of ligands can be measured in the presence and absence of receptor. Each measured log *D* value is a weighted average of the diffusion coefficients of receptor-bound and free ligand. Therefore, ligands with NMR signals that show increases in apparent molecular weight signify a receptor-bound population, whereas ligands that do not bind to the receptor exhibit no change in log *D*. This approach has previously been used to characterize the binding of a small protein receptor (hevein) to different oligosaccharides,[13] to detect the binding of plant extracts to the lectin domain of cholera toxin,[14] and to characterize the interactions of organic ligands in suspensions of titanium dioxide nanoparticles.[15]

In particular, pulsed field gradient NMR spectroscopy is an in situ methodology that enables the resolution of mixtures of different species in solution solely on the basis of their differentiated translational mobility. The use of 2D NMR experiments, which combine a chemical shift scale and a diffusion coefficient scale in so-called 2D diffusion-ordered (DOSY) NMR spectroscopy, provides a straightforward assignment of the diffusion correlation peaks associated with the various molecular species present in the mixture. This analytical tool is therefore complementary to conventional separation techniques,[16] such as size exclusion chromatography (SEC), in which the components of the mixture are separated chemically, rather than spectroscopically.

Figure 1 shows ^{1}H NMR spectra (500 MHz) of **1-All**, **1-S@Au**, and a mixture of **1-All** and **1-S@Au** in the presence of $CaCl_2$ (10 mM), whereas Figure 2 provides a representation of the corresponding 2D DOSY spectra. The diffusion coefficient is a property of the molecule as a whole and therefore shared by all the proton resonances of the molecule, so the signals of **1-All** are therefore spread out along a horizontal line with average log *D* values of 9.53. The solvent peak can be seen at 4.75 ppm, and log *D* = 8.76. Overlapping signals are expected to provide misplaced or distorted peaks, as is the case for one anomeric ^{1}H signal that overlaps with part of the solvent signal. This DOSY spectrum does not provide direct information about the molecular size, as the calibration of gradients, temperature, and sample viscosity effects were not fully ac-

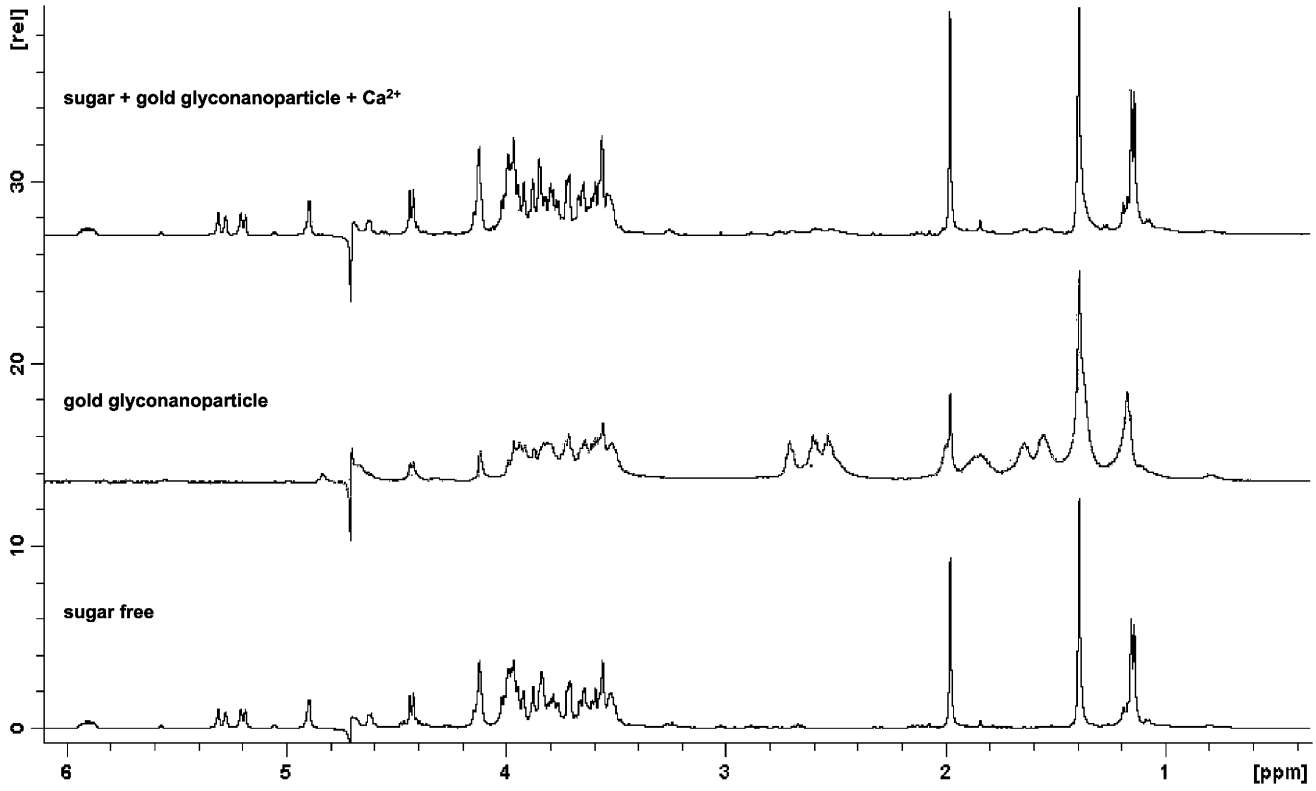

Figure 1. 1D ^{1}H NMR spectra (500 MHz) of **1-All** (bottom), **1-S@Au** (middle), and a mixture of **1-All** and **1-S@Au** (10:1, by weight, top) containing Ca^{II} ions.

counted for in this example. Trisaccharide system **1-S@Au** has a log *D* value around 10.1.

When the same DOSY experiment was carried out with a mixture of **1-All** and **1-S@Au** (10:1, by weight), without addition of Ca^{II} ions, no changes in the DOSY spectrum of **1-All** were observed, indicating that the carbohydrate–carbohydrate interaction, if present, should be very weak under these conditions. In the presence of an excess of Ca^{II} ions (10 mM $CaCl_2$), however, the log *D* values of the allyl resonances of **1-All** (see expansion in Figure 2 for clear evidence), which do not overlap with the **1-S@Au** resonances, changed substantially to an average value of log *D* = 9.78. Since the average log *D* value of **1-S@Au** was 10.10, the observed change, in between that measured for **1-All** and **1-S@Au**, indicates sugar binding to the GNP and thus Ca^{II}-mediated carbohydrate–carbohydrate interaction. The existence of several clustered units of the sugar (multivalency) seems to be required for the interaction to be observable. Indeed, an additional blank experiment with **1-All** and no **1-S@Au**, in the presence of Ca^{II} ions, did not show changes in the DOSY spectrum of the free trisaccharide. The DOSY experiment therefore allows the detection of a proportion of the carbohydrate–carbohydrate complex for this trisaccharide-trisaccharide@Au system.

In view of the success of the DOSY experiments for the pyruvated trisaccharide epitope, a similar approach was followed for the sulfated disaccharide moiety, which had been shown in TEM experiments to form large clusters of GNPs in the presence of Ca^{II} ions.[6] In this case, however, extreme line broadening of the signals did not allow the DOSY experiments to be performed. This line broadening can be correlated with a tight interaction under the experimental conditions and supports the existence of the previously reported strong disaccharide–disaccharide self-recognition.[5,6,8] It can be concluded that the success of the DOSY experiments in the case of the trisaccharide epitope is due to the weak-to-moderate affinity values of the employed system.

On the experimental side, the assays are essentially performed under equilibrium conditions. DOSY is a 2D experiment, collected as a series of 16–64 simple 1D ^{1}H experiments. Generally speaking, it requires less time to acquire DOSY data than it does for standard 2D NMR experiments such as correlation spectroscopy and nuclear Overhauser effect (NOE) spectroscopy. As mentioned above, disadvantages include the existence of overlapping NMR resonances, which make the evaluation of well separated signals necessary.

TR-NOESY-based studies

As previously shown for ligands that are not tightly bound and exchange between the free and the receptor-bound states at reasonably fast rates, the transferred nuclear Overhauser enhancement (TR-NOESY) experiment provides adequate means to detect binding.[12] As is illustrated in Figure 3, for the bound state, strong and negative NOE cross-peaks were only observed for **1-All** in the presence of **1-S@Au** under the experimental conditions described above for the DOSY experiments with Ca^{II} ions. This finding contrasts with those made for the free state (**1-All** with or without Ca^{II}) or in the presence of **1-**

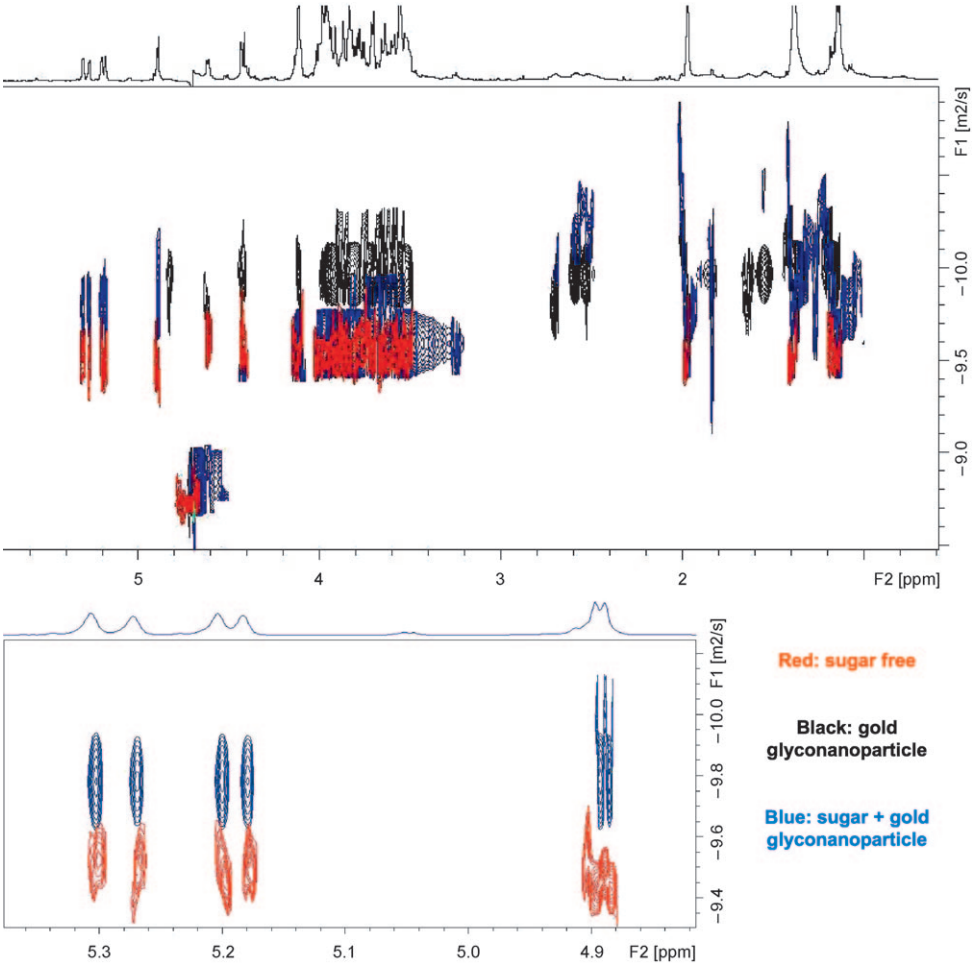

Figure 2. The DOSY spectra of **1-All** alone (red) and in the presence of **1-S@Au** (blue). The DOSY spectrum of the GNPs alone is also shown (black). Clear changes in the diffusion coefficient of the non-overlapping peaks of **1-All** between the free and bound states are observed when the GNPs and Ca^{II} ions are added to the NMR tube. No changes were evident when no Ca^{II} ions were present. An expansion of some non-overlapping proton resonances only present in **1-All** is shown at the bottom.

S@Au without Ca^{II}, for which NOE cross-peaks were weakly positive, further supporting Ca^{II}-mediated trisaccharide–trisaccharide@Au recognition.

The change in sign of the NOE cross-peaks indicates that the average tumbling rate of the trisaccharide under these experimental conditions is significantly slower than in the free state, which can be correlated with the existence of a molar fraction of trisaccharide molecules interacting with the trisaccharide-decorated nanoparticle, probably with mediation by Ca^{II} ions, because no change in sign was observed in the absence of these ions. Thus, like the DOSY technique,[15] the TR-NOESY experiment provides a suitable means to detect the possibly multivalent carbohydrate–carbohydrate interaction enhanced by the nanoparticle system.

STD experiments

As a final exercise, saturation transfer difference (STD) experiments were also attempted. The STD technique is also a straightforward NMR method that permits deduction of the existence of ligand–receptor binding.[11] In our case, however, no STD effects were observed in the trisaccharide signals upon irradiation of the protons of the linker. Since the kinetic requirements seem to be fulfilled by the system (TR-NOESY and DOSY experiments did work), there is probably not enough proton density[11] in the system to allow transfer of saturation from **1-S@Au** to interacting **1-All**, or the nanoparticle/sugar molar ratio was too low for the accumulative STD effect to take place.

Molecular dynamics simulation of the trisaccharide–trisaccharide complex in the presence of Ca^{II} ions

Although the role of Ca^{II} ions in homotopic-carbohydrate interactions is not yet understood at the molecular level, it can be inferred from our studies that Ca^{II} ions have an essential role in the approach and organization of the sugar moieties of the pyruvated trisaccharide.

With the aim of acquiring further insight into the interaction pattern, MD simulations were performed and putative 3D models of the carbohydrate-Ca^{II}-carbohydrate complexes were obtained.

The conformation of the trisaccharide as determined by MM/MD calculations

In a first step, potential energy maps for the constituent disaccharides were calculated.[17] Analysis of the distribution map of the Gal*p*4,6(*R*)Pyr(β1-4)Glc*p*NAc(β1- fragment reveals the presence of one major low-energy conformation and two local minima. The *syn*-Φ/*syn*-Ψ conformational family is the most populated, accounting for 92% of the population. This lowest-energy region is centered around $\Phi = 60^\circ$ and is defined by Ψ values between 90° and −90°. Small populations (about 8% total) of the *anti*-Φ and *anti*-Ψ conformations are also predicted. The calculations therefore suggest that in solution the Gal*p*4,6(*R*)Pyr(β1-4)Glc*p*NAc(β1- fragment behaves similarly around Φ/Ψ to lactose and *N*-acetyllactosamine.[18] For the Glc*p*NAc(β1-3)Fuc*p*(α1-fragment, similar behavior is found. According to the MM3* calculations, the global minimum is centered around $\Phi,\Psi = 60^\circ,0^\circ$. Minor populations (about 5% total)

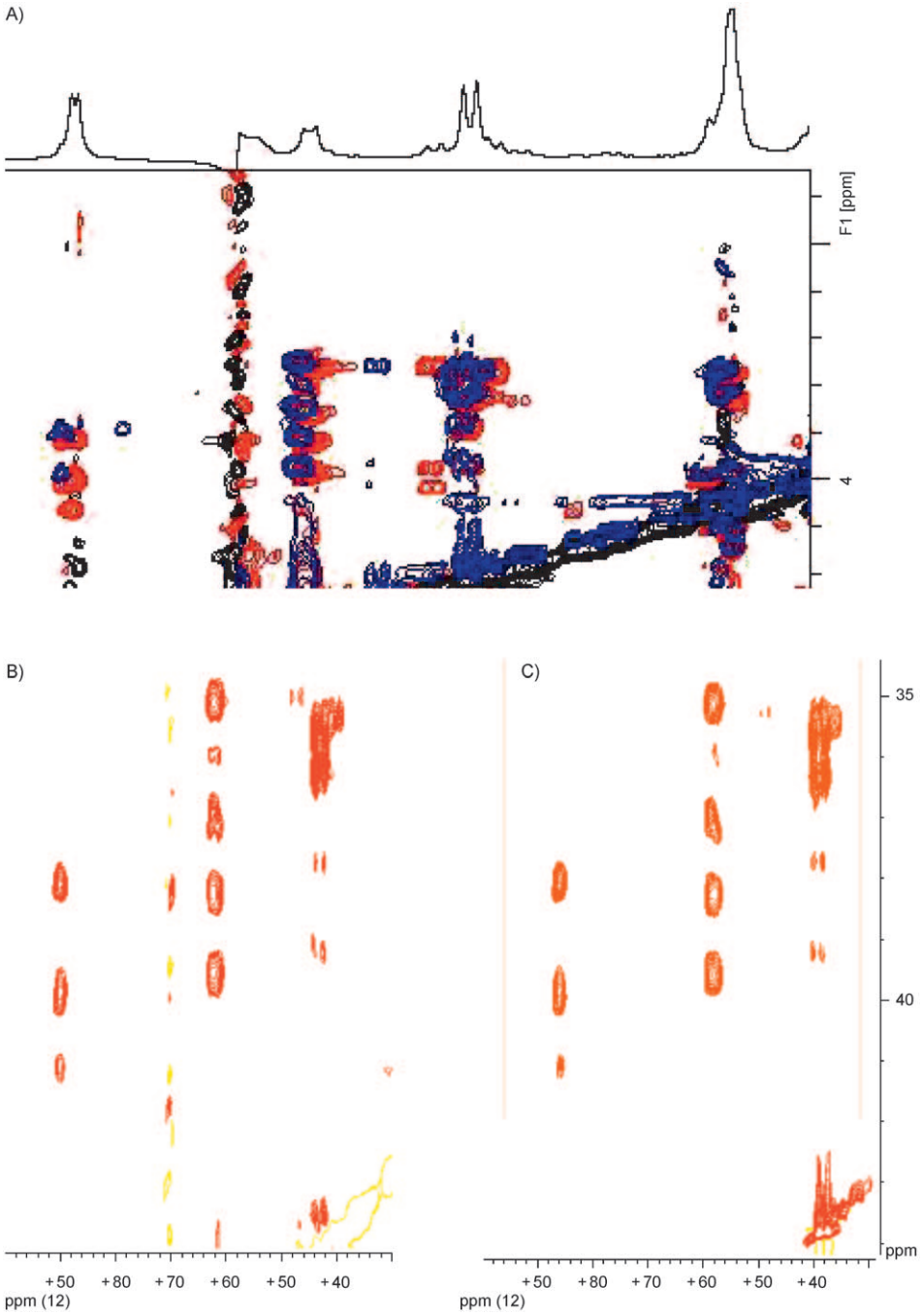

Figure 3. TR-NOESY spectra for **1-All** in the absence and in the presence of **1-S@Au** and $CaCl_2$. A) Superimpositions of different spectra are shown. The NOESY spectrum (400 ms mixing time) of **1-All** is shown in black (diagonal peaks) and red (cross-peaks). Cross-peaks and diagonal peaks have different signs, as would be expected for small molecules free in solution. In contrast, the cross-peaks in the presence of **1-S@Au** (blue) have the same sign as the diagonal peaks (also blue); thus, this indicates the interaction of **1-All** with **1-S@Au**. B) and C) The two experiments are shown separately. The cross-peaks are always given in red. For the free state (B), the diagonal peaks have different signs (yellow). For the bound state—that is for the **1-All**/**1-S@Au** system in the presence of Ca^{II} ions (C)—they show the same sign (also red); this showing the interaction process. When Ca^{II} ions are not present in solution, the spectrum is identical to that shown in Figure 3B. No NOEs different from those observed in the free state were observed, indicating that the pyruvated trisaccharide in the bound state shows the same conformational behavior as in the free state.

of the *anti-*Φ and *anti-*Ψ conformations are also calculated. Thus, on combining both fragments (Figure 4 and Figure S4 in the Supporting Information) it is possible to postulate a major conformation, which proved to be conformationally stable during a 5 ns MD simulation (Figure S3 in the Supporting Information) with only minor departures from the computed global minimum.

The conformation of the trisaccharide as determined by NMR spectroscopy

The validity of the theoretical results for **1-All** was verified by NMR spectroscopy. The ^{1}H NMR spectrum in D_2O was assigned through a combination of COSY, TOCSY, and HSQC experiments (Table 1). The intra-ring vicinal proton–proton coupling constants showed that the six-membered rings adopt either the $^4C_1$ (D) (Gal, GlcNAc) or $^1C_4$ (L) (Fuc) chair conformations (Figure 4 and Figure S4 in the Supporting Information).

Further structural information was extracted from NOESY and ROESY experiments to complement the MM3* data. The relevant inter-residue proton–proton distances in terms of the glycosidic and aglyconic angles for the major conformer A and for the distribution are collected in Table 2. For the Gal-GlcNAc moiety, it was calculated that H1-Gal is at a short distance from H4-GlcNAc in the *syn-*$\Phi\Psi$ conformers and from H3-GlcNAc in the *anti-*Ψ conformer, whereas H2-Gal is close to H4-GlcNAc in the *anti-*Φ geometry. In the NOE spectra, only the H1-Gal–H4-GlcNAc NOE was detected above the noise level; this demonstrates the existence of a very major conformer in solution (that is, at least qualitatively, the predominance of the *syn-*$\Phi\Psi$ orientation). Analogous reasoning was followed for the GlcNAc-Fuc moiety. Additionally, a more quantitative treatment was performed by comparing the distances obtained from MM calculations with those derived from the NOE intensities by a full relaxation matrix approach.[18,19]

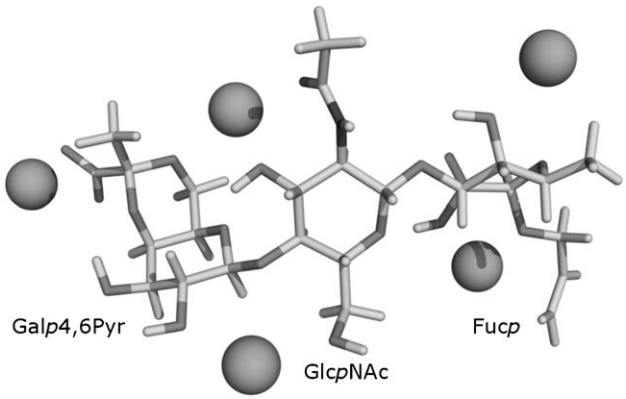

Figure 4. Minimized average 3D structure of **1-AII**, as derived from solvated MD simulation in the presence of 50 calcium ions. Five Ca^{II} atoms remain simultaneously coordinated along the MD simulation with the following sets of atoms: 1) carboxylate group, 2) At the bottom face O2-Gal and O6-GlcNAc, 3) O1-Fuc, O2-Fuc, and allyl group. 4) At the top face O4-Fuc, and endocyclic O-Fuc, and 5) O3-GlcNAc, carboxamide oxygen, and O6-Gal.

Table 1. ^{1}H NMR chemical shifts (δ, ppm) of **1-AII** in D_2O at 298 K.

	δ		δ		δ
H1-Gal	4.48	H1-GlcNAc	4.67	H1-Fuc	4.95
H2-Gal	3.62	H2-GlcNAc	3.77	H2-Fuc	3.86
H3-Gal	3.70	H3-GlcNAc	3.59	H3-Fuc	4.01
H4-Gal	4.18	H4-GlcNAc	3.77	H4-Fuc	3.89
H5-Gal	3.64	H5-GlcNAc	3.66	H5-Fuc	4.03
$H6^{ax}$-Gal	3.93	$H6^{a}$-GlcNAc	3.83	H6-Fuc	1.20
$H6^{eq}$-Gal	4.03	$H6^{b}$-GlcNAc	3.99		
Me-Gal	1.43	Me-GlcNAc	2.038		

Table 2. Relevant ensemble average ($\langle r^{-6}\rangle^{-1/6}$) proton–proton distances (Å) calculated for the MD simulations starting with the global minimum conformation (conformer A) of **1-AII**, together with a comparison between the expected NOEs for this MD-based distribution and those observed experimentally.

Proton pair	Distances $\Phi1/\Psi1(60/0)$ $\Phi2/\Psi2(60/0)$	NOE [%] expected (MD)	experimental
H1Gal-H4GlcNAc	2.4	9.3	9.2
H1Gal-H5Gal	2.4	10.6	10.2
H1GlcNAc-H5GlcNAc	2.4	10.3	9.8
H1GlcNAc-H4Fuc	2.5	7.4	8.2
H1GlcNAc-H3Fuc	2.6	6.7	6.5
H1Fuc-H2Fuc	2.5	5.8	5.9

In conclusion, it is clear (Table 2) that the agreement between the observed and the expected NOEs for the conformational distribution obtained from the MD simulations is more than satisfactory.

Molecular dynamics simulation of the trisaccharide–trisaccharide complex

MD simulations with explicit water were carried out in order to propose a model for the trisaccharide–trisaccharide self-recognition that was in agreement with the observed NMR data. Firstly, the geometry corresponding to the global minimum of **1-AII** resulting from the MM3* calculations (Figure 4 and Figure S4 in the Supporting Information) was simulated with MD and explicit water molecules. The structural details (ensemble average interproton distances and Φ/Ψ values) obtained were consistent with the experimental data reproducing the conformation inferred from NMR (see the Experimental Section for details of the MD simulations). Then, MD simulations, carried out with inclusion of 50 Ca^{II} ions in the water box, also led to a minimized average conformation for **1-AII**, in agreement with the NMR conformation described above. In principle, five different situations were deduced for this simple model, with five Ca^{II} atoms found to keep simultaneously coordinated with the following five sets of atoms (Figure 4): 1) carboxylate group, 2) O2-Gal and O6-GlcNAc, 3) O1-Fuc, O2-Fuc, and allyl group, 4) O4-Fuc and endocyclic O-Fuc, and 5) O3-GlcNAc, carboxamide oxygen, and O6-Gal. Each of these regions could, in principle, be able to accommodate one Ca^{II} ion, which is susceptible to coordination by a partner trisaccharide moiety.

In order to simulate the **1-AII**-Ca^{II}-**1-AII** complex, different possible means of sharing Ca^{II} atoms in dimeric models were considered. Coordination through the allyl group (defined above as set 3) was not considered because this situation does not occur in the native context. Furthermore, models with two trisaccharides sharing Ca^{II} through the sets defined as 4 and 5 were excluded for steric reasons, since major conflicts appear when it is attempted to set the second trisaccharide moiety. Only two models therefore remained to be studied: the first one with the participation of the carboxylate atoms belonging to set 1 (Figure 5), and the second one including interactions

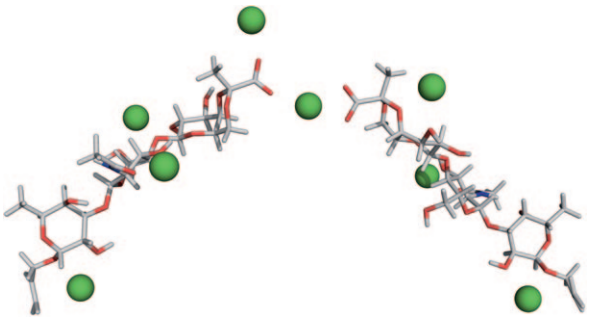

Figure 5. Minimized average 3D structure of the first putative model for establishing **1-AII**-Ca^{II}-**1-AII** interactions as derived from solvated MD simulation. One calcium ion bridges the two **1-AII** entities through the carboxylate moiety. The other possible ion binding sites have been kept for sake of clarity. No interaction was detected for non-pyruvated oligosaccharide, indicating the importance of this moiety for the interaction.

of atoms belonging to set 2 (O2-Gal and O6-GlcNAc; Figure 6). All the calcium–oxygen distances were within the expected ranges found in reported crystal structures of sugar–calcium complexes (2.30–2.65 Å[20]).

To provide models of the putative dimeric **1-AII** entities, the geometries shown in Figures 5 and 6 were subjected to MD simulations, with the Ca^{II} ions being kept at the two key sites.

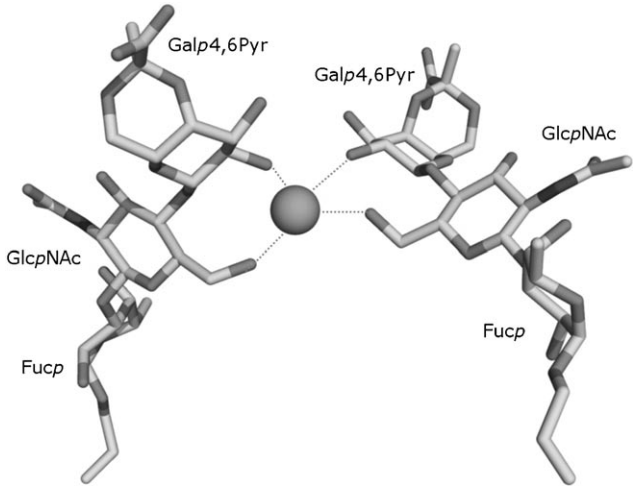

Figure 6. Minimized average 3D structure of the second putative model for establishing **1-All**-Ca^{II}-**1-All** interactions as derived from solvated MD simulation. One calcium ion bridges the two **1-All** entities through O2-Gal and O6-GlcNAc atoms at each sugar moiety.

Initial distance restrictions were applied after the equilibration period between the Ca^{II} ions and the putative coordinating atoms, finishing with unrestrained MD simulations. Ca^{II}-mediated coordination between the two units of sugar was maintained along the simulations for both starting geometries, as shown in Figures 5 and 6. These plausible models of the complexes provide interaction patterns that account for the existence of binding between the trisaccharides. Additionally, it should be pointed out that the two coordination models could co-exist in solution, weaving a network of carbohydrate–carbohydrate interactions in which Ca^{II} ions have a fundamental role in establishing and maintaining such a molecular recognition pattern. Figure 7, although merely speculative, shows two different perspectives of one of these possible 3D models that could account for the observed carbohydrate–carbohydrate interaction. As can be observed, the trisaccharides are gathered together by bridged calcium atoms, which preclude the dissociation of the complex. The different trisaccharide entities interact in a parallel fashion and are layered in pairs. They thus show a segmental type of interaction that can explain the actual interaction observed in nature for the native g-200, in which the polysaccharide–polysaccharide interaction takes place through the trisaccharide epitopes.

Conclusions

In conclusion, the employment of DOSY and TR-NOESY NMR experiments has proven to be useful for the study of weak carbohydrate–carbohydrate interactions and can be exploited for the understanding of other recognition processes, especially when ligand–receptor binding occurs with low to moderate affinity. Knowledge of the factors that drive such events, not only in the carbohydrate field but also in other bioorganic-related events, is crucial for understanding key processes that take place in nature.

Experimental Section

Pyruvated trisaccharide components: The synthesis of Gal*p*4,6(*R*)Pyr(β1–4)Glc*p*NAc(β1–3)Fuc*p*(α1-O)(CH_2CHCH_2) (**1-All**) and Gal*p*4,6(*R*)Pyr(β1–4)Glc*p*NAc(β1–3)Fuc*p*(α1-O)$(CH_2)_3S(CH_2)_6$-S@Au (**1-S@Au**) has been described recently.[8] The size of the gold nanoparticles amounts to 1.59 ± 0.5 nm (116 Au atoms), with a loading of on average 32 trisaccharide molecules per nanoparticle.

NMR spectroscopy: NMR experiments were recorded on a Bruker Avance instrument at 298 K. A concentration of about 0.5 mM **1-All** was used. Chemical shifts were referenced to external 2,2-dimethyl-2-silapentane-5-sulfonic acid (DSS) in D_2O. 1D spectra were acquired by use of 32 K data points, which were zero-filled to 64 K data points prior to Fourier transformation. COSY, TOCSY, HSQC, NOESY, and T-ROESY spectra (mixing times of 300, 400 and 500 ms) were acquired by standard techniques. Acquisition data matrices were defined by 1024×256 points, multiplied by appropriate window functions, and zero-filled to 1024×512 matrices prior to Fourier transformation. Baseline correction was applied in both dimensions. 1D-selective NOE spectra were also acquired at four

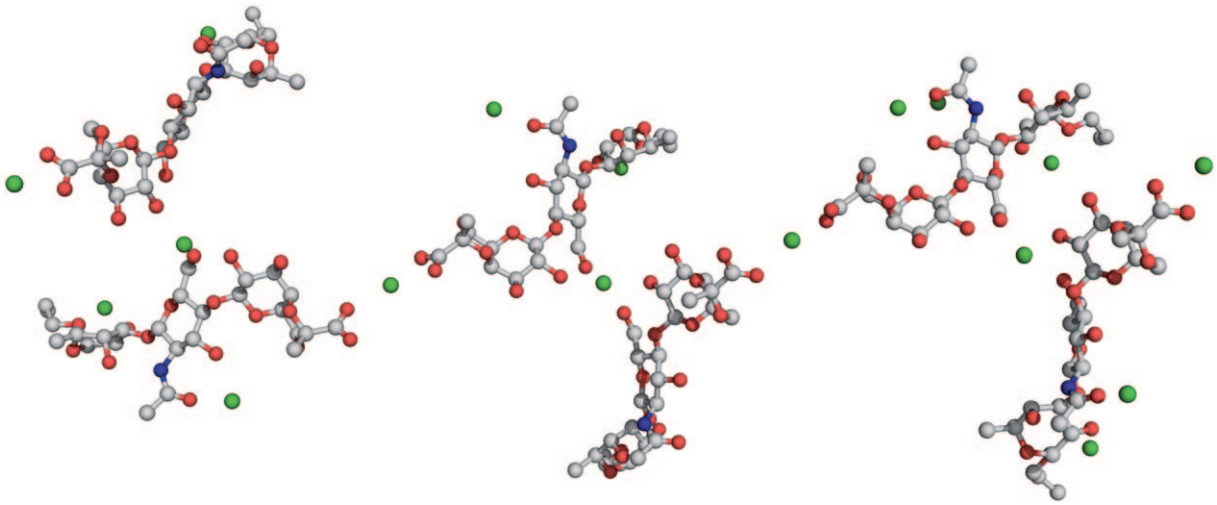

Figure 7. A putative extension of the interaction between the two **1-All** moieties that simultaneously uses both plausible Ca^{II} coordination sites.

different mixing times (200, 300, 400, and 500 ms). Spectra were processed with the aid of the Bruker XWIN-NMR program.

Distances were estimated from NOESY/ROESY experimental data as follows: NOE intensities were normalized with respect to the diagonal peak at zero mixing time. Selective T_1 measurements were performed on the anomeric and several other protons to obtain the values described above. Experimentally determined NOEs were fitted to a double exponential function, $f(t)=p0(e^{-p1t})(1-e^{-p2t})$ with $p0$, $p1$, and $p2$ being adjustable parameters.[21] The initial slope was determined from the first derivative at time $t=0$, $f'(0)=p0p2$. From the initial slopes, interproton distances were obtained by employing the isolated spin pair approximation.

Furthermore, the experimentally determined NOE intensities at a given mixing time were compared to those determined for single conformers or ensemble average distributions, calculated according to the complete relaxation matrix, automatically performed by a home-made program, which is available from the authors upon request.[19,22] Isotropic motion and external relaxation of 0.1 s^{-1} were assumed. A correlation time of 110 ps was used to obtain the best matching between experimentally measured and calculated NOEs for the intraresidue proton pairs H1-H3 and H1-H2 of the Gal and Fuc moieties, respectively.

DOSY: The standard Bruker protocol was used with a 500 MHz Avance spectrometer equipped with a broad-band *z*-gradient probe; 32 1D ^{1}H spectra were collected with a gradient duration of 2 ms and an echo delay of 100 ms for **1-AII**, or 250 ms for the **1-AII/1-S@Au** complexes. Acquisition times of about 16 and 32 min were required for the oligosaccharide samples and complexes, respectively. The ledbpg2s pulse sequence, with stimulated echo, longitudinal eddy current compensation, bipolar gradient pulses, and two spoil gradients, was run with a linear gradient (53.5 G cm^{-1}) stepped between 2% and 95%. The 1D ^{1}H spectra were processed and automatically baseline-corrected. The diffusion dimension, zero-filled to 1 k, was exponentially fitted according to pre-set windows for the diffusion dimension. To carry out the experiments with Ca^{II} ions, $CaCl_2$ (10 mM) was added to the same sample.

TR-NOESY: TR-NOESY experiments were recorded on a Bruker Avance 500 spectrometer at 298 K. Samples were prepared in D_2O. The concentration of **1-AII** was 0.5 mM, and the **1-AII/1-S@Au** ratio was about 10:1 (*w*/*w*). Mixing times of 250 and 400 ms were used. For the free state, only the 400 ms mixing time was employed. To carry out the experiments with Ca^{II} ions, $CaCl_2$ (10 mM) was added to the same sample.

Molecular mechanics calculations: Firstly, the trisaccharide was divided into its two disaccharide components: Gal*p*4,6(*R*)Pyr(β1–4)Glc*p*NAc(β- and Glc*p*NAc(β1–3)Fuc*p*(α1-. Relaxed ($\Phi\Psi$) energy maps for both fragments were then generated by systematic rotations around each glycosidic linkage and aglyconic bond with use of a grid step of 18°, optimization of the geometry at every $\Phi\Psi$ point by means of conjugate gradients iterations until the rms derivative was smaller than 0.05 kJ mol^{-1} $Å^{-1}$, and energy calculation with Macromodel and the MM3* force field[23] ($\varepsilon=80$) as integrated in the MAESTRO 7.5 package.[24] The *gg* and *gt* orientations of the GlcNAc unit were considered, because these have been shown to be much more stable than the alternative *tg* conformers. Two starting structures were thus considered for each disaccharide fragment, and in total 800 conformers were calculated. The probability distribution was calculated for each point according to a Boltzmann function at 298 K.

Molecular dynamics simulations: The molecular dynamics simulations were performed for **1-AII** by use of the MM3* force field with a dielectric constant of 80 within MAESTRO 7.5. For the MD simulations, several geometries corresponding to the combination of the different low-energy minima were used as input. A simulation temperature of 300 K was employed with a time step of 1.5 fs and an equilibration time of 100 ps. The total simulation time was 5 ns.

Molecular dynamics simulations in explicit water: Coordinates of the global minimum of **1-AII**, resulting from the above MM3* calculations, were used in the construction of the initial model. The pyruvate moiety was considered to be in the carboxylate state. Electrostatic potential-derived charges for the three non-standard monosaccharides were obtained by the RESP methodology[25] with a 6–31G* basis set as implemented in the Gaussian 98 program,[26] and GLYCAM-04[27] parameters were used to build the prep files. Systems including Ca^{II} cations were neutralized with the corresponding Cl^- anions. Each of the different starting geometries was immersed in a periodic water box that extended up to 10 Å away from any solute atom. Periodic boundary conditions were applied, and electrostatic interactions were represented by the smooth particle mesh Ewald method[28] with a grid spacing of 1 Å. Molecular dynamics simulations were carried out at 300 K and 1 atm with the SANDER module in AMBER 8.[29] SHAKE[30] was applied to all bonds involving hydrogens, and the integration time step was 2 fs. The simulation protocol consisted of a series of progressive energy minimizations followed by a 20 ps heating phase and a 250 ps equilibration period, after which a 2 ns unrestricted dynamics simulation was performed. For the two models considering one trisaccharide-trisaccharide complex sharing Ca^{II} atoms, the equilibration period was followed by a 250 ps restricted dynamics simulation (5 kcal mol^{-1} $Å^{-2}$) to maintain the Ca^{II} ions attached to the putative coordinating atoms. Finally, 1 ns of unrestricted dynamics simulation was performed for both models.

Acknowledgements

The group at CIB-CSIC thanks MEC/MCINN for financial support (Grant CTQ2006–10874-C02–01). S.M.-S. also thanks MEC for her Ramón y Cajal contract. The group at Utrecht University thanks the European Commission for financial support (Glycogold project; Contract No: MRTN-CT-2004–005645).

Keywords: carbohydrate–carbohydrate interactions · gold glyconanoparticles · *Microciona prolifera* · molecular dynamics · NMR spectroscopy

[1] M. W. Johansson, *Devel. Comp. Immunol.* **1999**, *23*, 303–315.
[2] X. Fernàndez-Busquets, M. M. Burger, *Cell. Mol. Life Sci.* **2003**, *60*, 88–112.
[3] a) G. N. Misevic, J. Finne, M. M. Burger, *J. Biol. Chem.* **1987**, *262*, 5870–5877; b) G. N. Misevic, M. M. Burger, *J. Biol. Chem.* **1993**, *268*, 4922–4929; c) U. Dammer, O. Popescu, P. Wagner, D. Anselmetti, H.-J. Güntherodt, G. N. Misevic, *Science* **1995**, *267*, 1173–1175; d) O. Popescu, G. N. Misevic, *Nature* **1997**, *386*, 231–232; e) X. Fernàndez-Busquets, M. M. Burger, *Microsc. Res. Tech.* **1999**, *44*, 204–218; f) J. Jarchow, J. Fritz, D. Anselmetti, A. Calabro, V. C. Hascall, D. Gerosa, M. M. Burger, X. Fernàndez-Busquets, *J. Struct. Biol.* **2000**, *132*, 95–105; g) C. Gourier, F. Pincet, E. Perez, Y. M. Zhang, J. M. Mallet, P. Sinay, *Glycoconjugate J.* **2004**, *21*, 165–174.
[4] a) D. Spillmann, K. Hård, J. Thomas-Oates, J. F. G. Vliegenthart, G. Misevic, M. M. Burger, J. Finne, *J. Biol. Chem.* **1993**, *268*, 13378–13387; b) D.

Spillmann, J. E. Thomas-Oates, J. A. van Kuik, J. F. G. Vliegenthart, G. Misevic, M. M. Burger, J. Finne, *J. Biol. Chem.* **1995**, *270*, 5089–5097.
[5] a) H. J. Vermeer, J. P. Kamerling, J. F. G. Vliegenthart, *Tetrahedron: Asymmetry* **2000**, *11*, 539–547; b) S. R. Haseley, H. J. Vermeer, J. P. Kamerling, J. F. G. Vliegenthart, *Proc. Natl. Acad. Sci. USA* **2001**, *98*, 9419–9424.
[6] a) A. Carvalho de Souza, K. M. Halkes, J. D. Meeldijk, A. J. Verkleij, J. F. G. Vliegenthart, J. P. Kamerling, *Eur. J. Org. Chem.* **2004**, 4323–4339; b) A. Carvalho de Souza, K. M. Halkes, J. D. Meeldijk, A. J. Verkleij, J. F. G. Vliegenthart, J. P. Kamerling, *ChemBioChem* **2005**, *6*, 828–831.
[7] A. Carvalho de Souza, J. P. Kamerling, *Methods Enzymol.* **2006**, *417*, 221–243.
[8] a) A. Carvalho de Souza, J. F. G. Vliegenthart, J. P. Kamerling, *Org. Biomol. Chem.* **2008**, *6*, 2095–2102;b) A. Carvalho de Souza, D. N. Ganchev, M. M. E. Snel, J. P. J. M. van der Eerden, J. F. G. Vliegenthart, J. P. Kamerling, *Glycoconjugate J.* **2008**, DOI: 10.1007/s10719-008-9196-7.
[9] a) J. M. de la Fuente, A. G. Barrientos, T. C. Rojas, J. Rojo, J. Cañada, A. Fernández, S. Penadés, *Angew. Chem. Int. Ed.* **2001**, *40*, 2258–2261; b) A. G. Barrientos, J. M. de la Fuente, T. C. Rojas, A. Fernández, S. Penadés, *Chem. Eur. J.* **2003**, *9*, 1909–1921; c) J. Rojo, V. Diaz, J. M. de la Fuente, I. Segura, A. G. Barrientos, H. H. Riese, A. Bernad, S. Penadés, *ChemBioChem* **2004**, *5*, 291–297; d) J. M. de la Fuente, P. Eaton, A. G. Barrientos, M. Menéndez, S. Penadés, *J. Am. Chem. Soc.* **2005**, *127*, 6192–6197; e) R. Ojeda, J. L. de Paz, A. G. Barrientos, M. Martín-Lomas, S. Penadés, *Carbohydr. Res.* **2007**, *342*, 448–459.
[10] a) A. Geyer, C. Gege, R. R. Schmidt, *Angew. Chem.* **1999**, *111*, 1569–1571; *Angew. Chem. Int. Ed.* **1999**, *38*, 1466–1468; b) A. Geyer, C. Gege, R. R. Schmidt, *Angew. Chem.* **2000**, *112*, 3381–3385; *Angew. Chem. Int. Ed.* **2000**, *39*, 3245–3249.
[11] B. Meyer, T. Peters, *Angew. Chem.* **2003**, *115*, 890–918; *Angew. Chem. Int. Ed.* **2003**, *42*, 864–890.
[12] "TR-NOESY Experiments", J. Jiménez-Barbero, T. Peters in *NMR Spectroscopy of Glycoconjugates* (Eds.: J. Jiménez-Barbero, T. Peters), Wiley, Weinheim, **2002**.
[13] P. Groves, M. Rasmussen, M. D. Molero, E. Samain, F. J. Cañada , H. Driguez, J. Jiménez-Barbero, *Glycobiology* **2004**, *14*, 451–456.
[14] M. Politi, J. Alvaro-Blanco, P. Groves, A. Prieto, J. A. Leal, F. J. Cañada, J. Jiménez-Barbero, *Eur. J. Org. Chem.* **2006**, 2067–2073.
[15] L. Van Lokeren, G. Maheut, F. Ribot, V. Escax, I. Verbruggen, C. Sanchez, J. C. Martins, M. Biesemans, R. Willem, *Chem. Eur. J.* **2007**, *13*, 6957–6966.
[16] P. Groves, M. Palczewska, M. D. Molero, G. Batta, F. J. Cañada, J. Jiménez-Barbero, *Anal. Biochem.* **2004**, *331*, 395–397.
[17] For a discussion of the application of molecular mechanics calculations to oligosaccharides, see: S. Pérez, A. Imberty, S. B. Engelsen, J. Gruza, K. Mazeau, J. Jiménez-Barbero, A. Poveda, J.-F. Espinosa, B. P. van Eyck, G. Johnson, A. D. French, M. L. C. E. Kouwijzer, P. D. J. Grootenhuis, A. Bernardi, L. Raimondi, H. Senderowitz, V. Durrier, G. Vergoten, K. Rasmussen, *Carbohydr. Res.* **1998**, *314*, 141–155.
[18] J. L. Asensio, J. Jiménez-Barbero, *Biopolymers* **1995**, *35*, 55–73.
[19] A. Poveda, J. L. Asensio, M. Martín-Pastor, J. Jiménez-Barbero, *J. Biomol. NMR* **1997**, *10*, 29–43.
[20] M. Dheu-Andries, S. Perez, *Carbohydr. Res.* **1983**, *124*, 324–332.
[21] F. Corzana, I. Cuesta, F. Freire, J. Revuelta, A. Bastida, J. Jiménez-Barbero, J. L. Asensio, *J. Am. Chem. Soc.* **2007**, *129*, 2849–2865, and references therein.
[22] M. Martín-Pastor, A. Canales, F. Corzana, J. L. Asensio, J. Jiménez-Barbero, *J. Am. Chem. Soc.* **2005**, *127*, 3589–3595.
[23] N. L. Allinger, Y. H. Yuh, J. H. Lii, *J. Am. Chem. Soc.* **1989**, *111*, 8551–8566.
[24] F. Mohamadi, N. G. J. Richard, W. C. Guida, R. Liskamp, M. Lipton, C. Caufield, G. Chang, T. Hendrickson, W. C. Still, *J. Comput. Chem.* **1990**, *11*, 440–451.
[25] P. Cieplak, W. D. Cornell, C. I. Bayly, P. A. Kollman, *J. Comput. Chem.* **1995**, *16*, 1357–1377.
[26] M. J. Frisch, G. W. Trucks, H. B. Schlegel, G. E. Scuseria, M. A. Robb, J. R. Cheeseman, V. G. Zakrzewski, J. A. Montgomery Jr., R. E. Stratmann, J. C. Burant, S. Dapprich, J. M. Millam, A. D. Daniels, K. N. Kudin, M. C. Strain, O. Farkas, J. Tomasi, V. Barone, M. Cossi, R. Cammi, B. Mennucci, C. Pomelli, C. Adamo, S. Clifford, J. Ochterski, G. A. Petersson, P. Y. Ayala, Q. Cui, K. Morokuma, D. K. Malick, A. D. Rabuck, K. Raghavachari, J. B. Foresman, J. Cioslowski, J. V. Ortiz, B. B. Stefanov, G. Liu, A. Liashenko, P. Piskorz, I. Komaromi, R. Gomperts, R. L. Martin, D. J. Fox, T. Keith, M. A. Al-Laham, C. Y. Peng, A. Nanayakkara, C. Gonzalez, M. Challacombe, P. M. W. Gill, B. G. Johnson, W. Chen, M. W. Wong, J. L. Andres, M. Head-Gordon, E. S. Replogle, J. A. Pople, *Gaussian 98*; Gaussian, Inc., Pittsburgh, PA, **1998**.
[27] K. N. Kirschner, R. J. Woods, *Proc. Natl. Acad. Sci. USA* **2001**, *98*, 10541–10545.
[28] T. A. Darden, D. York, L. G. Pedersen, *J. Chem. Phys.* **1993**, *98*, 10089–10092.
[29] D. A. Case, T. A. Darden, T. E. Cheatham, III, C. L. Simmerling, J. Wang, R. E. Duke, R. Luo, K. M. Merz, B. Wang, D. A. Pearlman, M. Crowley, S. Brozell, V. Tsui, H. Gohlke, J. Mongan, V. Hornak, G. Cui, P. Beroza, C. Schafmeister, J. W. Caldwell, W. S. Ross, P. A. Kollman, AMBER 8, University of California, San Francisco, **2004**.
[30] J. P. Ryckaert, G. Ciccoti, H. J. C. Berendsen, *J. Comput. Phys.* **1977**, *23*, 327–341.

Received: August 14, 2008
Published online on January 2, 2009

